# A Microfluidic Feed Forward Loop Pulse Generator for Molecular Communication

Yansha Deng*, Massimiliano Pierobon†, and Arumugam Nallanathan‡
*Department of Informatics, King's College London, London, UK
†Department of Computer Science and Engineering, University of Nebraska-Lincoln, Lincoln, Nebraska, USA
‡ School of Electronic Engineering and Computer Science, Queen Mary University of London, London, UK

***Abstract*—The design of communication systems capable of processing and exchanging information through molecules and chemical processes is a rapidly growing interdisciplinary field, which holds the promise to revolutionize how we realize computing and communication devices. While molecular communication (MC) theory has had major developments in recent years, more practical aspects in the design and prototyping of components capable of MC functionalities remain less explored. In this paper, motivated by a bulk of MC literature on information transmission via molecular pulse modulation, the design of a pulse generator is proposed as an MC component able to output a predefined pulse-shaped molecular concentration upon a triggering input. The chemical processes at the basis of this pulse generator are inspired by how cells generate pulse-shaped molecular signals in biology. At the same time, the slow-speed, unreliability, and non-scalability of these processes in cells are overcome with a microfluidic-based implementation based on standard reproducible components with well-defined design parameters. Mathematical models are presented to demonstrate the analytical tractability of each component, and are validated against a numerical finite element simulation. Finally, the complete pulse generator design is implemented and simulated in a standard engineering software framework, where the predefined nature of the output pulse shape is demonstrated together with its dependence on practical design parameters.**

## I. Introduction

The possibility of harnessing information processing and communication functionalities from chemical and physical processes at the level of molecules has been at the basis of a great bulk of research in recent years on Molecular Communication (MC) [1–4]. Despite substantial developments in the theoretical study of MC, the design and prototyping of components capable of MC functionalities has been a much less developed area, partly because of the highly interdisciplinary technical knowledge and tools required to practically engineer these systems.

In this paper, motivated by a bulk of MC literature on information transmission via molecular pulse modulation [5, 6], where a single or multiple types of molecules are emitted according to pulse-shaped signals to represent symbols in a digital message, we propose the design of a pulse generator component for MC systems. With reference to pulse generation in electrical systems, the proposed design generates molecular concentration pulses with a predefined shape according to an input trigger signal exclusively by means of chemical and physical processes in the molecular domain. The shape of the pulse is predictable a priori and reproducible as a function of component design parameters, thus potentially providing a platform for the definition of a standard pulse shape for MC [7].

The chemical processes at the basis of the proposed pulse generator are inspired by how cells process molecular signals in biology [8]. In particular, studies have revealed how a specific pattern of chained biochemical reactions underlying the regulation of cells' DNA expression, *i.e.*, gene regulatory network, results in the capability of generating pulse-shaped molecular concentration signals [9]. While the utilization of biological cells for molecular communication currently faces challenges such as slow speed, unreliability, and non-scalability [10], we propose a microfluidic-based implementation of the aforementioned chemical pattern based on standard reproducible components with well-defined design parameters.

The design of the proposed pulse generator is supported in this paper by both analytical and numerical simulation results. In particular, we present an analytical framework of the microfluidic components of the pulse generator based on convection-diffusion and the convection-diffusion-reaction equations in microfluidic systems, where input-output relations of each components, based on a 1D approximation of the microfluidic channels, are expressed as a function of design parameters, such as the length of each microfluidic channel, and the rates of the chemical reactions. These analytical results are validated against simulations performed through the COMSOL Multiphysics finite element solver. Finally, the complete pulse generator design is implemented and simulated in the COMSOL Multiphysics environment, where the dependence of different predefined output pulse shapes on the aforementioned design parameters is numerically evaluated.

The rest of the paper is organized as follows. In Sec. II we present the overall pulse generator design and motivate it in light of our abstraction of gene regulatory networks through a chemical reaction network in a microfluidic system. In Sec. III we detail and numerically evaluate the analytical models of the pulse generator components, while in Sec. IV we present the implementation and numerical simulation results of the overall design in COMSOL Multiphysics. Finally, in Sec. V we conclude the paper.

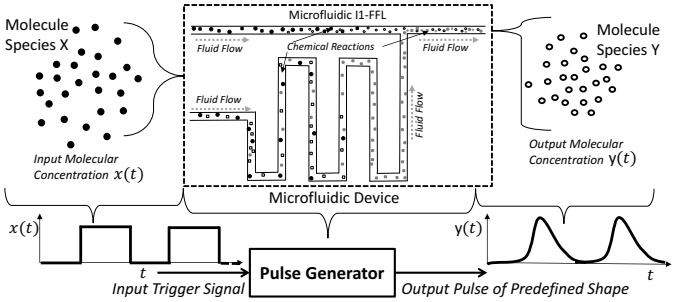


Fig. 1. Overall scheme of the proposed pulse generator for MC.

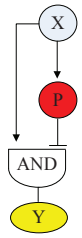


Fig. 2. The I1-FFL network motif.

## II. A Pulse Generator for Molecular Communication

The overall scheme of the proposed pulse generator for MC is shown in Fig. 1, where an input molecular signal composed of molecules of species $X$ in a fluid and concentration $x(t)$ as a function of the time $t$ is the input trigger of a microfluidic device that upon a variation in the concentration $x(t)$ produces as output another molecular signal composed of molecules of species $Y$ and concentration $y(t)$ that varies as a function of the time $t$ by following a predefined pulse shape. This pulse shape is dependent on the values of parameters in the microfluidic device implementation. As the fluid containing the molecules of species $X$ flows through the microfluidic device channels, a series of chemical reactions with other molecules generate the molecules of species $Y$ according to the aforementioned desired pulse signal. This microfluidic device design, detailed in Sec. II-C, is directly inspired by the incoherent type 1 feed forward loop motif in gene regulatory networks [10], described next.

### A. The FFL Motifs in Gene Regulatory Networks

Gene regulatory networks are sets of interconnected biochemical processes in a biological cell [11], where DNA genes are linked together by activation and repression mechanisms of certain biological macromolecules that regulate their expression into proteins. Each DNA gene contains coding sequences, which are chemical information for building proteins, and regulatory sequences, which are sites the proteins (transcription factor) can bind and control the rate of the gene expression, either by increasing (activation) or decreasing (repression) the rate of protein synthesis. In gene regulatory networks, genes are interconnected such as the proteins produced by one or more genes regulate the expression of one or more genes, thus resulting in complex protein expression dynamics.

Gene regulatory networks can be abstracted with nodes representing the genes, interconnected by directed edges that correspond to the control of a gene (edge destination) expression by a transcription factor encoded by another gene (edge source). Network motifs are patterns of nodes and directed edges that occur more frequently in natural gene transcription networks than randomized networks [8]. The FFL is a family of network motifs among all three-node patterns frequently observed in nature [8, 9]. In the structure of FFL, the transcription factor protein $X$ regulates the genes expressing other two proteins, namely, $P$ and $Y$, where $P$ is also a transcription factor that regulates the gene expressing protein $Y$. Depending on the types of these regulations, either activation or repression, there are 8 different of FFLs [10].

Among other FFLs found in nature, the Incoherent type 1 FFL (I1-FFL) results in a pulse-like dynamics of its output $Y$ [9]. As shown in Fig. 2, an input gene expresses the protein $X$, which is a transcription factor for the genes expressing $Y$ and $P$. In presence of $X$, the expression of the genes encoding protein $Y$ and protein $P$ are activated, resulting in the build up of the concentrations of protein $Y$ and protein $P$, respectively. On its turn, the protein $P$ is another transcription factor that works as a repressor for the gene encoding protein $Y$. The AND input to the gene that encodes $Y$ corresponds to a situation where this gene is activated when the transcription factor $X$ binds to the regulatory sequence, but it is inactivated whenever transcription factor $P$ binds to the same sequence independently from the presence of X. In such a way, protein $X$ initializes the rapid expression of the gene encoding protein $Y$ first, and after a delay, enough $P$ accumulates and represses the production of protein $Y$, whose concentration will continuously decrease because of natural degradation. This generates a pulse shape for the concentration of protein $Y$ as a function of the time.

One example of I1-FFL is the galactose system of *E. coli*, where the galactose utilization operon (a cluster of genes sharing the same regulatory sequences and expressed together) $gal$ETK is regulated in an I1-FFL by the activator $CRP$ (X), and the repressor $GalS$ (P) [12]. Results shown that in nature we can observe a pulse-like expression of the $gal$ETK genes, which is initiated by a step variation of active $CRP$ mediated by the molecular species $cAMP$ ($S_x$).

In this paper, we take inspiration from the I1-FFL to design a pulse generator in the molecular domain. Although the discipline of synthetic biology is opening the road to the programming of functionalities in the biochemical environment through genetic engineering of biological cells [13], there are a number of factors that encouraged an alternative technology for the design of a pulse generator in this paper, such as the small number of molecules involved for each cell together with difficulties in coordinating multiple cells, the added complexity of cellular behavior, including cell growth, evolution, and biological noise, and the slow response time of

genetic regulatory networks such as the I1-FFL, whose output pulse shape is usually realized in nature in the order of cell generation time (hours) as indicated in [12, Fig. 4].

### *B. An I1-FFL-inspired Chemical Reaction Network*

Inspired by the I1-FFL mechanism in gene regulation networks, we explore the realization of I1-FFL via mass action chemical reactions, *i.e.*, processes that convert one or more input molecules (*reactants*) into one or more output molecules (*products*). Reactions may proceed in forward or reverse directions, which are characterized by forward ($k_f$) and reverse ($k_r$) reaction rates, respectively. Within the scope of this paper, we assume unbalanced reactions where the forward reaction rate is much greater than the reverse rate. A chemical reaction network is defined as a finite set of reactions involving a finite number of species [14], where these reactions occur in a well-stirred environment, aiming to realize a function or algorithm via mass action chemical reactions. Specific chemical reaction networks have already been designed for signal restoration, noise filtering, and finite automata, respectively, through a discipline known as molecular programming [15].

To execute the same functionality of an I1-FFL with a chemical reaction network, we define three chemical reactions as follows:

$$\text{Reaction I}: X + S_y \rightarrow Y, \tag{1}$$

$$\text{Reaction II}: X + S_p \rightarrow P, \tag{2}$$

$$\text{and Reaction III}: Y + P \rightarrow Z, \tag{3}$$

where these reactions involve the input molecular species $X$, the molecular species $S_p$, and $S_y$, and intermediate product molecular species $P$, and the output molecular species $Y$.

In the I1-FFL gene regulation network, the active $X$ first activates the gene expressing the protein $Y$, and only when $P$ accumulates sufficiently, it suppresses the expression of the protein $Y$, generating the aforementioned pulse-like concentration signal. Here, the molecular species $X$, $S_p$, and $S_y$ are only injected at $t = 0$, and the chemical reactions in (1), (2), and (3) happen simultaneously with a much quicker speed under well-stirred environment than that of the I1-FFL gene regulation network dynamics, which may not result in the pulse-like output signal $Y$ when these three reactions have the same reaction rate. One way to cope with it is to adjust the reaction rate to be different among these reactions.

However, in practice, we want to design the molecular communication system with the pulse-like output triggered by the squared pulse input representing bit-1 transmission. In such a way, the output pulse only occurs inside the duration of a squared pulse input, and every bits are modulated to their corresponding pulses as shown in Fig. 1. To control the squared pulse input signals, the sequence of each reaction, and the delayed arrival of product $P$ after Reaction II in (2), we propose a microfluidic device to realize the same functionality of I1-FFL as in gene regulation network in Fig. 3 and containing the reactions (1), (2), and (3).

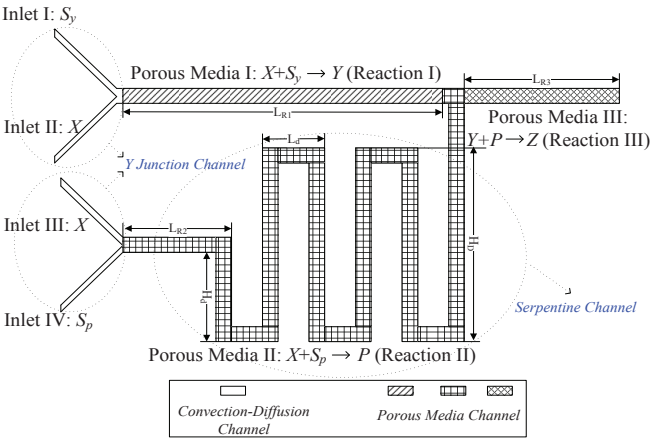


Fig. 3. Novel Microfluidic Device for Pulse Generation.

### *C. Microfluidic Device Design*

In this subsection, we describe each component of our proposed microfluidic device, with reference to Fig. 3 and the aforementioned chemical reaction network. A microfluidic device is a system that can process or manipulate small ($10^{-9}$ to $10^{-18}$ litres) amount of fluids using channels in dimensions of tens to hundreds of micrometres [16]. Recently, an increasing number of biological and chemical experiments are conducted in microfluidic or labs-on-a-chip (LOC) devices, due to inherent advantages in miniaturization, integration, portability and automation with low reagents consumption, rapid analysis, and high efficiency [17].

*1) Y Junction:* The reactions between reactants require mixing to occur in a short distance, which can be facilitated by diffusion in Y junctions. Y junctions are configured by one outlet and two inlets, *i.e.*, Y junction I and Y-junction II in Fig. 3, where the angle between the main channel and the first inlet starting anticlockwise from the main channel is $45^o$, which tends to be the standard in microfluidics. Fluid flows are infused at each branch of the Y-junction by means of a syringe pump, which can be described by a square pulse signal, as in Fig. 1, with the width equal to the length of injection time $T_{\text{ON}}$.

The fluid flow containing input reactant $X$ with concentration $C_{X_0}$ is injected into the Inlet II and Inlet III with velocity $v$ using syringe pumps during the injection time $T_{\text{ON}}$, whereas the reactant $S_y$ with concentration $C_{y_0}$ and reactant $S_p$ with concentration $C_{p_0}$ are continuously injected into Inlet I and Inlet IV, respectively. By doing so, the flows from Inlet I and Inlet IV can flush the microfluidic device continuously without influencing Reaction III in (3).

*2) Reacting Flow in Porous Media:* A porous medium is realized by partitioning the total volume into solid (*e.g.* a sponge or bundles of capillaries) matrix and pore space, where the pore space is filled by the flow. The mechanical processes responsible for mixing the reactants in porous media are advection and diffusion, which facilitate the occurrence of chemical reactions.

The outflow of Y-junction I passes through the porous media Channel I with length $L_{R1}$ to realize the Reaction I in (1) to generate the output signal $Y$, and the outflow of Y-junction II passes through the porous media Channel II with length $L_{R2}$ to realize the Reaction II (2) to generate $P$. Once $P$ arrives at the porous media Channel III with length $L_{R3}$, Reaction III (3) occurs to decrease the output signal $Y$.

*3) Convection-Diffusion Channel:* Except from these three porous media channels, the four inlet channels are convection-diffusion channels for continuous flow, detailed in Sec. III-B.

*4) Serpentine Channel:* After propagation through the porous media Channel II, the serpentine channel is designed to delay the arrival of $P$ in a compact space within the microfluidic device, with the result of delaying the contact between product protein $P$ and output protein $Y$, therefore delaying the Reaction III. The maximum length of the serpentine channel is denoted as $L_d$, and the maximum and the minimum height of the serpentine channel are denoted as $H_D$ and $H_d$, respectively. The design in Fig. 3 is conventionally denoted as containing 2 delay lines, due to its two bended tubes with peak height $H_D$ in the serpentine channel.

## III. Analytical Model of the Microfluidic Device Components

In this section, we first describe the basic characteristics of microfluidic channel, and then provide the analytical model for each main component of the proposed microfluidic device to reveal their dependency on design parameters.

### A. Basic Characteristics of Microfluidic Channel

The scaling law is introduced to reveal the physical properties of microsystems, which expresses the variation of physical quantities with size $l$ of the microsystems with time, and minimal pressure variance. The scaling law of two classes of forces is expressed as [18]

$$\frac{\text{surface forces}}{\text{volume forces}} \propto \frac{l^2}{l^3} \to \infty, (l \to 0). \tag{4}$$

This scaling law reveals that the volume forces become negligible compared with surface forces, when scaling down to microscale, such as in a microfluidic device.

In physics, the motion of viscous fluid flow inside microfluidic channels is described by the Navier-Stokes equation as [19]

$$\rho\left(\frac{\partial \mathbf{u}}{\partial t}\right) + \rho\left(\mathbf{u}\cdot\nabla\right)\mathbf{u} = -\nabla p + \mu\nabla^2\mathbf{u} + \mathbf{F}, \tag{5}$$

where $\nabla$ is Nabla vector differential operator, $\mathbf{u}$ is the fluid velocity field, $\rho$ is the density of the liquid in the order of $10^3$ $\mathrm{kg/m^3}$, $p$ is the pressure, $\mathbf{F}$ is the external force per unit mass, and $\mu$ is the constant viscosity of the liquid. This equation relates the velocity to the pressure.

Usually, the Navier-stoke equations are very complicated to solve in closed form. Luckily, they can be simplified, and its analytical solutions can be obtained in some special cases, such as incompressible fluid ($\nabla\cdot\mathbf{u} = 0$), steady flow (all changes of fluid properties with time are zero), and laminar flow ( $(\mathbf{u}\cdot\nabla)\mathbf{u} = 0$). The flow where the turbulence is not exhibited is called laminar flow: in this case, the fluid velocity field and the velocity field gradient are orthogonal, and the flow is unidirectional throughout an infinite channel [20].

The nature of the flow highly depends on the Reynolds number, which is the most famous dimensionless parameter in fluid mechanics. For flow in a pipe, the Reynolds number is defined as [18]

$$\mathrm{Re} = \frac{\rho u D_H}{\mu}, \tag{6}$$

where $D_H$ is the hydraulic diameter of the pipe, and $u$ is the area-averaged velocity of the fluid ($\mathrm{m/s}$).

The Reynolds number captures the ratio of the inertia force on an element of fluid to the viscous force on the same element. For large Reynolds number, the viscous forces are small relative to inertia forces. For very small Reynolds number ($\mathrm{Re} \ll 1$), the viscous forces are dominant compared with the inertia force. In a microfluidic channel, the hydraulic diameter of the pipe and the area-averaged velocity of the fluid are relatively small, as such, the fluid flows are mostly at very low Reynolds number ($\mathrm{Re} < 1$), and the inertia force, such as gravity and turbulence, is negligible [21, 22].

### B. Analytical Approximation for Microfluidic Component

In a microfluidic channel, it is noted that when the distance $l$ from the inlet of channel and the pipe radius $r$ follows $l/r \gg \mathrm{Re}$, the laminar flow can be treated as a unidirectional flow, and the infinite channel analysis can be used for the analysis of finite length channel [18, 23].

To capture the dispersion of a moving fluid in the microfluidic channel, we first present the analytical model of the convection-diffusion channel with unidirectional flow and constant average velocity throughout the length of the flow field.

*1) Convection-Diffusion Channel:* For a semi-infinite medium with source point $x = 0$, the convection-diffusion channel is characterized by [24]

$$D\frac{\partial^2 C(x,t)}{\partial x^2} - v\frac{\partial C(x,t)}{\partial x} = \frac{\partial C(x,t)}{\partial t}, \tag{7}$$

where $D$ is the diffusion coefficient, $v$ is the average velocity of the fluid, and $C(x,t)$ is the molecular concentration in the fluid.

The molecules are injected continuously at the source of channel $x = 0$, thus the first initial boundary condition is

$$C(0,t) = C_0; t \geq 0. \tag{8}$$

At $t = 0$, the molecular concentration in any positions is zero, thus the second initial boundary condition is

$$C(x,0) = 0; x \geq 0. \tag{9}$$

The concentration at locations far away from the source equals zero, thus the third boundary condition is

$$C(\infty,t) = 0; t \geq 0. \tag{10}$$

By taking into account the boundary conditions in (8), (9), (10), we can solve the convection-diffusion equation in (7) following [25], and derive the molecular concentration as

$$C\left(x,t\right)=\frac{C_0}{2}\left[\text{erfc}\left(\frac{x-vt}{2\sqrt{Dt}}\right)+e^{\frac{vx}{D}}\text{erfc}\left(\frac{x+vt}{2\sqrt{Dt}}\right)\right]. \quad (11)$$

*2) Convection-Diffusion-Reaction Channel:* To quantitatively describe the chemical reaction and dispersion of chemical species in the porous media of the microfluidic device, we introduce the one-dimensional convection-diffusion-reaction equation. Since the second-order reactions occur in the porous media, and the species $S_p$ and $S_y$ are continuously supplied and abundant, we can assume there is no significant change in the concentration of the species $S_p$ and $S_y$ throughout the process, and they can be approximated as time-invariant constants.

For the microfludic porous media device with low Reynolds number (Re$\ll$1), its convective-dispersive equation with chemical reaction $X+S_y\rightarrow Y$ is described as

$$D\frac{\partial^2 C_X(x,t)}{\partial x^2}-v\frac{\partial C_X(x,t)}{\partial x}=\frac{\partial C_X(x,t)}{\partial t}+k_1C_X(x,t)C_{S_y}, \quad (12)$$

$$D\frac{\partial^2 C_Y(x,t)}{\partial x^2}-v\frac{\partial C_Y(x,t)}{\partial x}=\frac{\partial C_Y(x,t)}{\partial t}-k_1C_X(x,t)C_{S_y}, \quad (13)$$

where $k_1$ is the reaction rate.

The species $X$ is injected at the inlet of the microfludic device $x=0$, thus the first initial boundary condition is

$$C_X(0,t)=C_{X_0};t\geq 0\Rightarrow C_X(0,t)=C_{X_0}u\left(t\right). \quad (14)$$

At $t=0$, the concentration of species $X$ in any positions is zero, thus the second initial boundary condition is

$$C_X(x,0)=0;x\geq 0. \quad (15)$$

The concentration change over locations far away from the source equals zero, thus the third boundary condition is

$$\frac{\partial C_X(\infty,t)}{\partial x}=0;t\geq 0. \quad (16)$$

The solution can be obtained by taking the Laplace transform of Eqs. (12), (14), and (15) using

$$\widetilde{C}_X\left(x,s\right)=\int_0^\infty e^{-st}C_X\left(x,t\right)dt. \quad (17)$$

The Laplace transform of (12) satisfying (15) is

$$D\frac{\partial^2\widetilde{C_X}(x,s)}{\partial x^2}-v\frac{\partial\widetilde{C_X}(x,s)}{\partial x}=\left(s+k_1C_{S_y}\right)\widetilde{C_X}(x,s). \quad (18)$$

The Laplace transform of (14) and (16) are

$$\widetilde{C_X}(0,s)=\frac{C_0}{s}, \quad (19)$$

and

$$\frac{\partial\widetilde{C_X}(\infty,s)}{\partial x}=0. \quad (20)$$

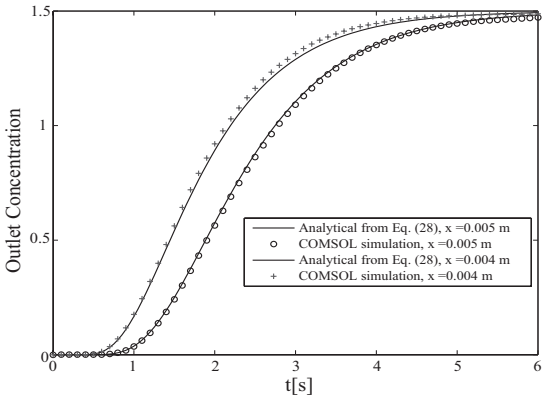


Fig. 4. Outlet concentration of $Y$ in the convection-diffusion-reaction channel.

Combining (17), (18), and (20), we derive

$$\widetilde{C_X}(x,s)=\frac{C_0}{s}\exp\left[\frac{vx}{2D}-x\sqrt{\frac{v^2}{4D^2}+\frac{s+k_1C_{S_y}}{D}}\right]. \quad (21)$$

Taking the inverse Laplace transform of (21), we derive

$$\begin{aligned}C_X(x,t)=&\frac{C_0}{2}\left\{\exp\left[\frac{(v-\alpha)\,x}{2D}\right]\text{erfc}\left[\frac{x-\alpha t}{2\sqrt{Dt}}\right]\right.\\&\left.+\exp\left[\frac{(v+\alpha)\,x}{2D}\right]\text{erfc}\left[\frac{x+\alpha t}{2\sqrt{Dt}}\right]\right\}, \quad (22)\end{aligned}$$

where $\alpha=\sqrt{v^2+4k_1C_{S_y}D}$.

To derive the concentration of species $Y$, we combine (12) and (13) as

$$D\frac{\partial^2 C_s(x,t)}{\partial x^2}-v\frac{\partial C_s(x,t)}{\partial x}=\frac{\partial C_s(x,t)}{\partial t}, \quad (23)$$

where $C_s(x,t)=C_X(x,t)+C_Y(x,t)$. Interestingly, this equation becomes the convection-diffusion equation.

The sum concentration of $X$ and $Y$ follows the three boundary conditions

$$C_s(0,t)=C_0;t\geq 0, \quad (24)$$

$$C_s(x,0)=0;x\geq 0, \quad (25)$$

$$C_s(\infty,t)=0;t\geq 0. \quad (26)$$

Following the same derivations in Sec. III-B1, we have the solution for (23) under the above boundary conditions as

$$C_s\left(x,t\right)=\frac{C_0}{2}\left[\text{erfc}\left(\frac{x-vt}{2\sqrt{Dt}}\right)+e^{\frac{vx}{D}}\text{erfc}\left(\frac{x+vt}{2\sqrt{Dt}}\right)\right]. \quad (27)$$

Taking the deduction of $C_X(x,t)$ in (22) from $C_s\left(x,t\right)$ in (27), we derive the concentration of $Y$ as

$$\begin{aligned}C_Y\left(x,t\right)=&\frac{C_0}{2}\left\{\text{erfc}\left(\frac{x-vt}{2\sqrt{Dt}}\right)+e^{\frac{vx}{D}}\text{erfc}\left(\frac{x+vt}{2\sqrt{Dt}}\right)\right.\\&-\exp\left[\frac{(v-\alpha)\,x}{2D}\right]\text{erfc}\left[\frac{x-\alpha t}{2\sqrt{Dt}}\right]\\&\left.-\exp\left[\frac{(v+\alpha)\,x}{2D}\right]\text{erfc}\left[\frac{x+\alpha t}{2\sqrt{Dt}}\right]\right\}, \quad (28)\end{aligned}$$

where $\alpha = \sqrt{v^2 + 4k_1 C_{S_y} D}$.

In Fig. 4, we plot the analytical concentration of species $P$ in (28) with parameters $C_{X_0} = 1.5$ mol/m$^3$, $k_1 = 10^3$m$^3$/mol/s, and $D_X = D_{S_y} = D_Y = 1 \times 10^{-6}$m$^2$/s. The simulation points in Fig. 4 are plotted from the outlet molecular concentration of species $Y$ in a porous media with reaction $X + S_y \rightarrow Y$, which happens throughout the square microfluidic tube with $d = h = 10^{-5}$m in a COMSOL Multiphysics finite element simulation, where the molecular concentration of $X$ ($C_{X_0} = 1.5$ mol/m$^3$) is injected at the inlet of the microfluidic tube with velocity $v = 0.002$m/s. As can be seen, the simulation points are in precise agreement with the analytical curves. The outlet concentration of $Y$ increases and reaches the maximum due to the high reaction rate $k_1$. Furthermore, the longer the microfluidic tube, the slower the increase in the outlet concentration of $Y$, and the lower the overall output concentration of $Y$.

*3) Y Junction Channel:* In our design, the Y junction channel is an important interconnection configuration for combining two channels. The species $X$ and the species $S_p$ are injected into the two inlets of the Y junction channel at $x = 0$ with the same velocity $v$. As the length of the subchannel is much smaller than that of the combined channel, and no reaction happens in the Y junction channel, injecting the same volume and concentration of independent species $X$ or $S_p$ into two subchannels can be treated as diluting species $X$ using $S_p$, or diluting species $S_p$ using $X$. Thus, the outlet concentration of $X$ or $S_p$ in Y junction can be approximately equivalent to that of a straight channel as in (11), with half of the inlet concentration.

*4) Serpentine Channel:* In our design, the serpentine channel is used to delay the arrival time of species $P$, where the number of delay lines determines the length of this delay [26, 27]. The turning channel in the delay lines usually causes different fluid laminas propagating with different lengths. However, when the channel is in low Reynolds number with very small side length tube, we can approximate the outlet concentration of the delay lines channel as that of a straight channel with equivalent length.

## IV. Numerical Results

In this section, we provide a numerical evaluation of the proposed microfluidic device for pulse generation.

### A. COMSOL Multiphysics Implementation

To examine the pulse generation characteristics of our proposed pulse generator in Fig. 3, we implement the aforementioned design in COMSOL according to the geometry in Fig. 5, with different numbers of delay lines in the four subfigures. In Fig. 5, these four subfigures are with the same geometry parameters as in Table I except the serpentine channel in Table II. Reacting flows in the porous media module of COMSOL are utilized to implement the the chemical Reactions I, II, and III. We also assume diffusion coefficient for each species as $D = 10^{-6}$m$^2$/s, the velocity for each inlet channel as $v = 0.002$m/s, the reaction rate for each reaction as $k_1 = 0.66971$m$^3$/mol/s, and the initial concentration as $C_{X_0} = 4$mol/m$^3$, $C_{S_{p_0}} = 4$mol/m$^3$, and $C_{S_{y_0}} = 3$mol/m$^3$.

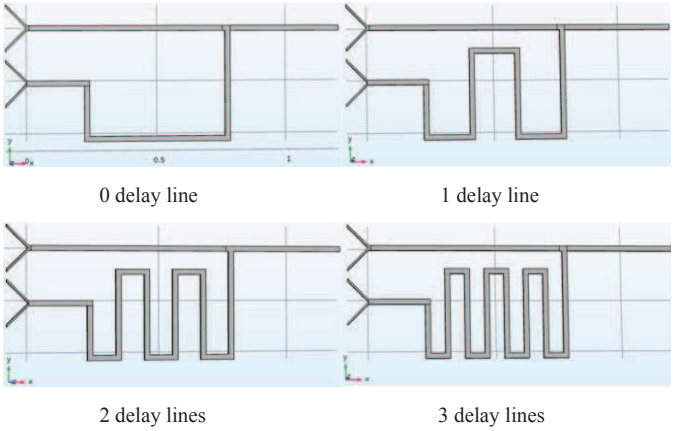


Fig. 5. Four delay lines.

TABLE I
The Parameters of Proposed Microfluidic Design.

| Channel | Length ($\mu$m) | Width ($\mu$m) | Depth ($\mu$m) |
|---|---|---|---|
| Inlet Y junction | $80\sqrt{2}$ | 10 | 10 |
| Outlet Y junction Porous media I | 1200 | 20 | 10 |
| Outlet Y junction Porous media II | 240 | 20 | 10 |
| Porous media I channel | 740 | 20 | 10 |
| Porous media III channel | 420 | 20 | 10 |

TABLE II
The Parameters of Serpentine Channel in Fig. 5.

| Channel | $L_d$ ($\mu$m) | $H_D$ ($\mu$m) | $H_d$ ($\mu$m) |
|---|---|---|---|
| 0 delay line | 560 | 0 | 210 |
| 1 delay line | 220 | 350 | 210 |
| 2 delay lines | 128 | 350 | 210 |
| 3 delay lines | 97 | 350 | 210 |

### B. Pulse Shaping

In Fig. 6, we plot the inlet concentration of $X$ and the outlet concentration of $Y$ versus time for the four microfludic designs in Fig. 5. The input signal is a square pulse-like signal generated by a syringe pump with concentration $C_{X_0}$, here normalized to one, and duration as 2s. It is interesting to see that the output pulses can be generated successfully during the ON input signal, and the tail of pulse decays to zero during the OFF input period, in less than 0.2s. We also notice that increasing the number of delay lines increases the maximum concentration of output signal $Y$, which is due to the later arrival of $P$ at the porous media Channel III, resulting from the increased length of the serpentine channel, gives more time for Reaction I to generate $Y$. It is seen that the longer the serpentine channel, the wider the generated pulse, because of the longer time given to generate $Y$ in Reaction I, and the more $Y$ that needs to be consumed in Reaction III.

These observations showcase that the number of delay lines in serpentine channel can be well-designed to shape the pulse.

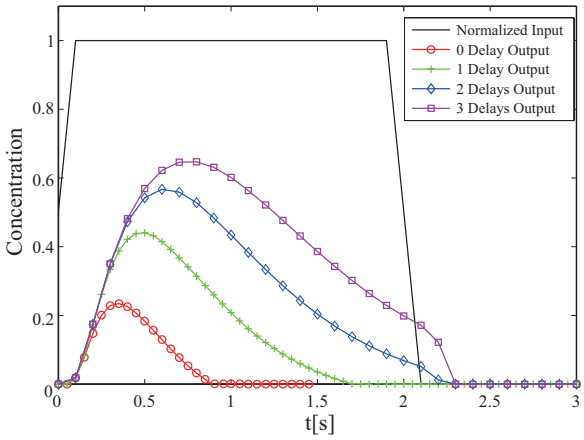


Fig. 6. Concentration of input and output signals in FFL-inspired microfluidic device versus time.

The narrow pulses generated by 0&1 delay lines in the serpentine channel may reduce the intersymbol interference during the receiver detection, whereas the wide pulses generated by 2&3 delay lines in the serpentine channel result in stronger received signal, with a pulse shape that more precisely covers the ON time of the input signal.

## V. Conclusion

In this paper, we proposed a pulse generator for MC capable of generating a predefined pulse-shaped molecular concentration upon a triggering input. The design of this pulse generator is motivated by the MC literature on information transmission via molecular pulse modulation, and it is inspired on a motif in cells' gene regulatory networks. The proposed design is based on a microfluidic system with standard and reproducible components, whose design parameters control the shape of the output pulse. Analytical expressions of these components are provided and numerically validated to demonstrate their input-output dependency on standard design parameters, while a simulation-based implementation of the overall design shows how the predefined shaping of the pulse can be controlled at design phase. We envision not only that this pulse generator might be an important components in the design of future MC systems, but also that the methodology presented in this paper will help in the design of additional MC components inspired by biochemical processes and based on microfluidic systems.

## Acknowledgment

This work was supported by the US National Science Foundation (NSF) through grant MCB-1449014, and the NSF Nebraska EPSCoR through the First Award grant EPS-1004094.

## References

[1] I. F. Akyildiz, F. Brunetti, and C. Blazquez, "Nanonetworks: A new communication paradigm at molecular level," *Computer Networks (Elsevier) Journal*, vol. 52, no. 12, pp. 2260–2279, August 2008.

[2] I. F. Akyildiz, M. Pierobon, S. Balasubramaniam, and Y. Koucheryavy, "The internet of bio-nano things," *IEEE Communications Magazine*, vol. 53, no. 3, pp. 32–40, March 2015.

[3] N. Farsad, H. B. Yilmaz, A. Eckford, C.-B. Chae, and W. Guo, "A comprehensive survey of recent advancements in molecular communication," *IEEE Communications Surveys & Tutorials*, vol. 18, no. 3, pp. 1887–1919, Third Quarter 2016.

[4] Y. Deng, A. Noel, W. Guo, A. Nallanathan, and M. Elkashlan, "Stochastic geometry model for large-scale molecular communication systems," in *Proc. IEEE GLOBECOM*, Dec. 2016.

[5] E. B. Pehlivanoglu, B. D. Unluturk, and O. B. Akan, "Modulation in molecular communications: A look on methodologies," in *Modeling, Methodologies and Tools for Molecular and Nano-scale Communications*. Springer International Publishing, 2017, pp. 79–97.

[6] Y. Deng, A. Noel, W. Guo, A. Nallanathan, and M. Elkashlan, "Analyzing large-scale multiuser molecular communication via 3D stochastic geometry," *IEEE Trans. Mol. Biol. Multi-Scale Commun.*, 2017.

[7] IEEE P1906.1/D2.0, *IEEE Draft Recommended Practice for Nanoscale and Molecular Communication Framework*. IEEE Standards, 2015.

[8] R. Milo, S. Shen-Orr, S. Itzkovitz, N. Kashtan, D. Chklovskii, and U. Alon, "Network motifs: simple building blocks of complex networks," *Science*, vol. 298, no. 5594, pp. 824–827, Oct. 2002.

[9] U. Alon, "Network motifs: theory and experimental approaches," *Nature Reviews Genetics*, vol. 8, no. 6, pp. 450–461, Jun. 2007.

[10] A. Uri, *An introduction to systems biology: design principles of biological circuits*. CRC press, 2006.

[11] G. Karlebach and R. Shamir, "Modelling and analysis of gene regulatory networks," *Nature Reviews Molecular Cell Biology*, vol. 9, no. 10, pp. 770–780, Oct. 2008.

[12] S. Mangan, S. Itzkovitz, A. Zaslaver, and U. Alon, "The incoherent feed-forward loop accelerates the response-time of the gal system of escherichia coli," *Journal of molecular biology*, vol. 356, no. 5, pp. 1073–1081, Mar. 2006.

[13] L. J. Kahl and D. Endy, "A survey of enabling technologies in synthetic biology," *Journal of Biol. Eng.*, vol. 7, no. 1, p. 13, May 2013.

[14] M. Cook, D. Soloveichik, E. Winfree, and J. Bruck, "Programmability of chemical reaction networks," in *Algorithmic Bioprocesses*. Springer, 2009, pp. 543–584.

[15] T. H. Klinge, "Modular and robust computation with deterministic chemical reaction networks," Ph.D. dissertation, 2016.

[16] G. M. Whitesides, "The origins and the future of microfluidics," *Nature*, vol. 442, no. 7101, pp. 368–373, Jul. 2006.

[17] X. J. Li and Y. Zhou, *Microfluidic devices for biomedical applications*. Elsevier, 2013.

[18] H. Bruus, "Theoretical microfluidics. 2008."

[19] R. Temam, *Navier-stokes equations*. North-Holland Amsterdam, 1984, vol. 2.

[20] F. M. White and I. Corfield, *Viscous fluid flow*. McGraw-Hill New York, 2006, vol. 3.

[21] D. Di Carlo, "Inertial microfluidics," *Lab on a Chip*, vol. 9, no. 21, pp. 3038–3046, Sep. 2009.

[22] D. Di Carlo, D. Irimia, R. G. Tompkins, and M. Toner, "Continuous inertial focusing, ordering, and separation of particles in microchannels," *Proc. Natl. Acad. Sci.*, vol. 104, no. 48, pp. 18 892–18 897, Nov. 2007.

[23] B. J. Kirby, *Micro-and nanoscale fluid mechanics: transport in microfluidic devices*. Cambridge University Press, 2010.

[24] T. Stocker, *Introduction to climate modelling*. Springer Science & Business Media, 2011.

[25] Y. Deng, A. Noel, M. Elkashlan, A. Nallanathan, and K. C. Cheung, "Modeling and simulation of molecular communication systems with a reversible adsorption receiver," *IEEE Trans. Mol. Biol. Multi-Scale Commun.*, vol. 1, no. 4, pp. 347–362, Jul. 2016.

[26] X.-D. Wang, X.-X. Zhang, T. Liu, Y.-Y. Duan, W.-M. Yan, and D.-J. Lee, "Channel geometry effect for proton exchange membrane fuel cell with serpentine flow field using a three-dimensional two-phase model," *J. Fuel Cell. Sci. Tech.*, vol. 7, no. 5, p. 051019, Jul. 2010.

[27] J. Feser, A. Prasad, and S. Advani, "On the relative influence of convection in serpentine flow fields of pem fuel cells," *J. Power Sources*, vol. 161, no. 1, pp. 404–412, Oct. 2006.